Modeling and Computation of Propagating Waves from Coronary Stenoses

H.T. Banks,[*] J.H. Barnes,[†] A. Eberhardt,[‡] H. Tran,[§] S. Wynne[¶]

August 15, 2000

Abstract

The ability to reliably detect coronary artery disease based on the acoustic noises produced by a stenosis can provide a simple, non-invasive technique. Current research exploits the shear wave fields in body tissue to detect and analyze coronary stenosis. A mathematical model of this system couples the generation of these acoustic noises with the propagation of the sound and shear waves through the chest cavity. In our initial investigations we consider a one-dimensional, homogeneous viscoelastic model. A quasi-linear viscoelastic stress-strain relationship was proposed by Fung [8] for a variety of biological tissues. Though an effective model, this formulation presents significant computational difficulties in dynamic situations. We present several alternate constitutive relations, based on an internal variable formulation, that approximate Fung's constitutive relation well when optimized. More importantly, results from the corresponding dynamic models match well with simulated data of wave propagation through a homogeneous soft tissue-like gel.

Mathematics Subject Classification: 65M32, 74D10, 74J30

Keywords and Phrases: Propagating shear waves, nonlinear viscoelastic materials, inverse problems.

1 Introduction

Coronary artery disease (CAD) is the buildup of plaque (cholesterol, calcium, and platelets) in the inner wall of coronary arteries known as stenosis in which

---
[*] Center for Research in Scientific Computation, Box 8205, North Carolina State University, Raleigh, NC 27695-8205

[†] MedAcoustics Inc,5540 Centreview Drive, Suite 114, Raleigh, NC 27606

[‡] MedAcoustics Inc,5540 Centreview Drive, Suite 114, Raleigh, NC 27606

[§] Center for Research in Scientific Computation, Box 8205, North Carolina State University, Raleigh, NC 27695-8205

[¶] Center for Research in Scientific Computation, Box 8205, North Carolina State University, Raleigh, NC 27695-8205

Report Documentation Page		*Form Approved* *OMB No. 0704-0188*

1. REPORT DATE **15 AUG 2000**	2. REPORT TYPE	3. DATES COVERED **00-00-2000 to 00-00-2000**
4. TITLE AND SUBTITLE **Modeling and Computation of Propagating Waves from Coronary Stenoses**		5a. CONTRACT NUMBER
		5b. GRANT NUMBER
		5c. PROGRAM ELEMENT NUMBER
6. AUTHOR(S)		5d. PROJECT NUMBER
		5e. TASK NUMBER
		5f. WORK UNIT NUMBER
7. PERFORMING ORGANIZATION NAME(S) AND ADDRESS(ES) **North Carolina State University,Center for Research in Scientific Computation,Raleigh,NC,27695-8205**		8. PERFORMING ORGANIZATION REPORT NUMBER
9. SPONSORING/MONITORING AGENCY NAME(S) AND ADDRESS(ES)		10. SPONSOR/MONITOR'S ACRONYM(S)
		11. SPONSOR/MONITOR'S REPORT NUMBER(S)
12. DISTRIBUTION/AVAILABILITY STATEMENT **Approved for public release; distribution unlimited**		
13. SUPPLEMENTARY NOTES		
14. ABSTRACT **see report**		
15. SUBJECT TERMS		

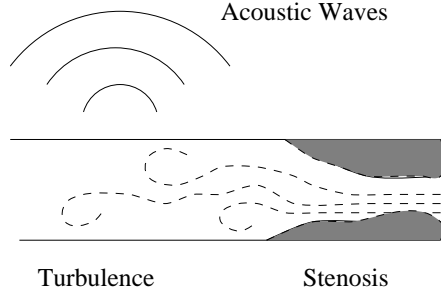| 16. SECURITY CLASSIFICATION OF:			17. LIMITATION OF ABSTRACT	18. NUMBER OF PAGES	19a. NAME OF RESPONSIBLE PERSON
a. REPORT **unclassified**	b. ABSTRACT **unclassified**	c. THIS PAGE **unclassified**		**21**	

Figure 1: Turbulent blood flow generated by a stenosis.

blood flow is restricted and the oxygen supply to the heart muscle is decreased. The end result of arterial stenosis is permanent damage to the heart muscle. It is estimated that CAD affects more than 12 million people in the United States, and it is the single leading cause of death and premature permanent disability [2]. As such, the detection and treatment of CAD is a high priority.

It is well known that arterial stenoses produce sounds due to turbulent blood flow in partially occluded arteries (see e.g., [1] or [27]). In principle, turbulent normal wall forces exist at and downstream from arterial stenosis. These wall forces, which are extremely small, exert a pressure on the wall of the artery, which then causes a small displacement in the surrounding soft tissue (see Figure 1). The vibrations of the surrounding body tissues, which occur in two forms, a compressional wave and a shear wave, produce sounds [23], [27]. In larger arteries such as the carotid arteries, these acoustic sounds can be detected by physicians using a stethoscope. However, detecting acoustic signals in smaller arteries deep inside the body has proved difficult for two reasons: these acoustic noises attenuate significantly as they travel through the intervening tissues [23], and, moreover, many complex sounds within the body can overwhelm conventional acoustic detection systems.

Current detection techniques include the angiogram which is a reliable, yet expensive, invasive technique and prone to interobserver variability (see e.g., [9], [17]). Ultra-fast CT techniques are also employed; this is a non-invasive imaging technique effective in detecting and scoring the severity of calcium deposits in the coronary arteries. CT testing equipment is very expensive. However, the biggest limitation is that the method only detects calcium deposits and not the soft plaques that make up many of the most dangerous lesions.

The ability to reliably detect coronary artery disease based on the acoustic noises can provide a simple, non-invasive approach [18]. Current research exploits the shear wave fields in body tissue to detect and analyze coronary

2

stenosis [15]. At low frequencies (<2 kHz), shear wave attenuation and wave propagation speed is low, which proves useful for studying propagation characteristics and estimating mechanical properties of tissue-like media. Recent techniques measure the shear wave propagation at the surface of the chest wall using a multiple array of sensors. Phased array signal processing is then used to image the underlying volume and locate stenosis sites within the coronary tree.

A complete mathematical model for this acoustic wave system couples two separate processes: (1) the generation of the sound and shear waves at the arterial stenosis and transmission through the arterial wall, and (2) the propagation of the sound, or shear waves, through the chest cavity to the external acoustic sensors. Modeling the wave propagation through the chest cavity is a nontrivial task. It is well accepted that body soft tissue medium behaves like a viscoelastic medium [8]. In addition, the acoustic waves will travel through ribs and at least two sorts of tissue: lung tissue and muscular connective tissue. These spatial inhomogeneities in the propagating medium cause spatial changes in the medium's propagation speed. These variations induce refractive effects, which bend the rays along which the wave propagates and ultimately leads to multi-paths.

In this paper we address the second process: the shear wave propagation through a viscoelastic, heterogeneous medium. To start, however, we first analyze the most simple case, i.e., a one-dimensional, homogeneous viscoelastic model for which experimental data is readily available. The corresponding physical model is depicted in Figure 2; the synthetic gel has material properties similar to those of soft tissues and the tube mimics an arterial vein with stenosis.

The motion of a viscoelastic body is governed by the laws of conservation of mass and momentum, the stress-strain (constitutive) relations, plus boundary and initial conditions. A quasi-linear viscoelastic stress-strain relationship which captures well the viscoelastic characteristics for a variety of biological tissues was proposed by Fung [8] for soft tissues. The constitutive relation incorporates a continuous spectrum of relaxation times into the model, and gives the stress in terms of a Boltzmann integral which depends on the history of the elastic response rate. Though effective in modeling quasi-static creep and relaxation, this formulation presents significant computational difficulties in dynamic situations.

In an effort to avoid some of these computational challenges, we investigate the effectiveness of using alternative stress-strain formulations to model time dependent shear wave propagation through a homogeneous medium. We will present several simple formulations that, when optimized, approximate well Fung's constitutive relation. More importantly, results from the corresponding dynamic models match well with simulated data of wave propagation through a homogeneous soft tissue-like gel.

The organization of the paper is as follows. We first develop the model equations in Section 2. In Section 3 we introduce alternative stress-strain constitu-
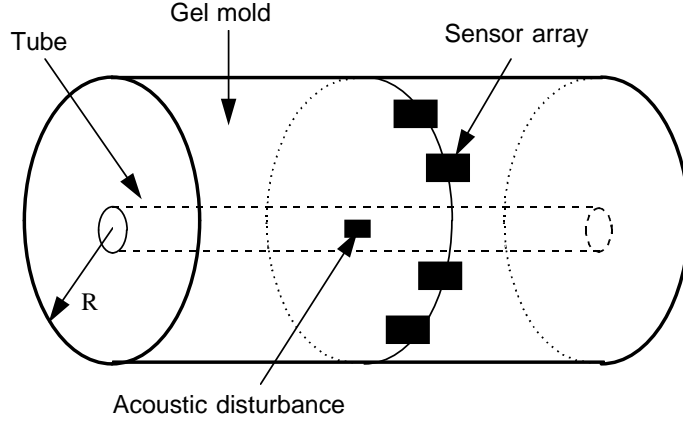
Figure 2: The 1D homogeneous viscoelastic model.

tive relations and compare with Fung's formulation. The physical and dynamic models are given in Section 4, and we discuss the computational method for integrating the models in Section 5. In Section 6 we present model simulations and compare with data, and follow with conclusions in Section 7.

2 Model Formulation

We first develop the one dimensional model equations based on Newton's law of motion, the principle of conservation of mass, and laws of thermodynamics. In the following, let u, σ, and X denote the Cartesian shear displacement, shear stress, and body force per unit volume, respectively. Let ρ denote the mass density and v denote the shear velocity $\partial u/\partial t$. X is a source term for the acoustic sound propagation.

From the conservation of mass, we have the continuity equation

$$\frac{\partial \rho}{\partial t} + \frac{\partial}{\partial x}(\rho v) = 0. \tag{1}$$

Conservation of momentum implies that

$$\frac{\partial \rho v}{\partial t} + \frac{\partial}{\partial x}(\rho v^2) = \frac{\partial \sigma}{\partial x} + X.$$

Using equation (1) in the left side of the above equation, we have the Eulerian

4

equation of motion of a continuum

$$\rho \left(\frac{\partial v}{\partial t} + v \frac{\partial v}{\partial x} \right) = \frac{\partial \sigma}{\partial x} + X.$$

Since we are interested in only small displacements, we ignore the higher order term $\rho v \partial v / \partial x$ to obtain

$$\rho \frac{\partial^2 u}{\partial t^2} = \frac{\partial \sigma}{\partial x} + X. \tag{2}$$

We next obtain a constitutive equation that relates stress and strain, and eventually stress and displacement. The medium of interest is soft tissue (arteries, muscle, skin, lung, etc...) which is considered viscoelastic material. That is, soft tissue exhibits the characteristics of creep (a slow progressive deformation of a material under constant stress), relaxation (a gradual decrease of stress when the material is held at constant deformation), and hysteresis (the stress-strain curve in the loading process is usually different than in the unloading process).

The quasi-linear relation proposed by Fung [8] describes the quasi-static behavior of many biological soft tissues (see, e.g., [5],[10],[11], [19],[20],[21],[25], [28],[29],[30]). This relation between stress and strain in simple elongation is given by

$$\sigma(t) = \int_0^t G(t - \tau) \frac{d\sigma_e(\lambda(\tau))}{d\tau} \, d\tau. \tag{3}$$

where $G(t)$ and $\sigma_e(\lambda(\cdot))$ are the reduced relaxation function and the elastic response, respectively. Here, the relaxation function is assumed to be separable in time and strain.

By definition, the elastic response is the tensile stress instantaneously generated in the tissue when a step function of stretching λ is imposed on the specimen. For many materials, it may be approximated by

$$\frac{d\sigma_e}{d\lambda} = \alpha(\sigma_e + \beta), \quad \sigma_e(1) = 0, \tag{4}$$

where α and β are constants to be estimated from data. For a justification of this approximation, see [8], p. 279. We recall [3], [8] that the stretch ratio λ is related to the infinitesimal strain ϵ (and displacement u) by the equation

$$\lambda^2 = 1 + 2E_{11} = \left(1 + \frac{\partial u}{\partial x} \right)^2 = (1 + \epsilon)^2.$$

Solving equation (4) for σ_e, we then have

$$\sigma_e(\lambda(t)) = -\beta + \beta e^{\alpha \partial u / \partial x}. \tag{5}$$

The reduced relaxation function proposed by Fung is given by

$$G(t) = \left\{ 1 + C \left[E_1(\frac{t}{\tau_2}) - E_1(\frac{t}{\tau_1}) \right] \right\} \left[1 + c \ln \left(\frac{\tau_2}{\tau_1} \right) \right]^{-1} \tag{6}$$

5

where $E_1(z)$ is the exponential integral function defined by

$$E_1(z) = \int_z^\infty \frac{e^{-t}}{t} \, dt.$$

The parameters C, τ_1, and τ_2 are constants determined from data; the constant C represents the degree to which viscous effects are present, τ_1 and τ_2 represent the fast and slow viscous time phenomena, respectively [22]. Fung's formulation provides a continuous spectrum of relaxation. This is a departure from other models that commonly express the relaxation function as the sum of exponential functions where each exponent is identified with the rate constant of a relaxation mechanism, i.e.,

$$G(t) = \frac{\sum C_i e^{-\nu_i t}}{\sum C_i}.$$

According to Fung, such a model will have discrete relaxation rate constants and corresponds to a discrete hysteresis spectrum; this is incompatible with the observation that, for many biological soft tissues, the hysteresis loop is nearly independent of the strain rate within several decades of the rate variation.

Equations (2), (3), (5), and (6) comprise an integro-differential system. In summary, the one-dimensional equations for wave propagation through a homogeneous, viscoelastic medium are the equation of motion (2) and Fung's stress-strain relation (3) with the elastic response and reduced relaxation function defined by (5) and (6), respectively. Because the constitutive equation (3) is in integral form with a complicated kernel described by equation (6), it must be approximated computationally. This requires the storage of the history of the kernel function $G(t)$ in small time increments. Furthermore, this time discretization might be considerably smaller than the time discretization used in the approximation of the equation of motion (2) (so that the errors in computing the constitutive equation do not contribute to the errors in approximating the acoustic energy). This is especially true in the case where the elastic response σ_e is highly oscillatory, as in our study here. For computational efficiency, we propose alternatives to Fung's constitutive equation in the following section.

3 Constitutive Law Formulations and Comparisons

In this section we propose three computationally tractable alternatives to Fung's quasi-linear constitutive equation for soft tissues and compare them numerically to Fung's formulation. The idea is to consider internal variable models (Maxwell solids in differential form) as in [12] and, more recently, in investigations of nonlinearities and hysteresis arising from a class of magnetorheological-based smart elastomers [3], [4]. The basic assumption is that one has a finite number

of "internal strain" variables, $\epsilon_j(t), j = 1, \ldots, N$, driven by the infinitesimal strain $\epsilon(t) = \lambda(t) - 1$. In this formulation the stress is given by

$$\sigma(t) = \sum_{i=1}^{N} \epsilon_j(t). \tag{7}$$

The internal strains can be modeled dynamically as

$$\frac{d\epsilon_j(t)}{dt} = -\nu_j \epsilon_j + C_j \frac{d\sigma_e}{dt}(\lambda(t)), \qquad j = 1, \ldots, N. \tag{8}$$

Using the variation of constants formula, solutions to the above system of differential equations with zero initial conditions, $\epsilon_j(0) = 0$, are given by

$$\epsilon_j(t) = \int_0^t C_j e^{-\nu_j (t-s)} \frac{d}{ds} \sigma_e(\lambda(s)) ds, \qquad j = 1, \ldots, N. \tag{9}$$

Note that the internal variable approach (7) is equivalent to the integral formulation (3) with an exponential form for the reduced relaxation function, i.e., $G(t) = \sum_{i=1}^{N} C_j e^{-\nu_j t}$. The difference in these two formulations is only in their numerical implementation: using (3) one deals with numerical approximation of an integral function without any consideration of internal dynamics, whereas using the internal variable approach (7) one has to numerically solve a decoupled system of differential equations. Computationally, one expects that the internal variable model approach is much more efficient in terms of both speed and data storage.

More generally, the internal strains might be modeled by nonlinear dynamics of the form

$$\frac{d\epsilon_j(t)}{dt} = g_j(\epsilon_j(t)) + C_j \frac{d\sigma_e}{dt}(\lambda(t)), \quad j = 1, \ldots, N. \tag{10}$$

However, this formulation cannot be written in Boltzmann form.

We will compare Fung's constitutive relation (3) with several constitutive relations resulting from the internal variable approach. Let $N = 1$ in (7), then $\sigma(t) = \epsilon_1(t)$, $G(t) \approx C_1 e^{-\nu_1 t}$, and σ is obtained as the solution of the following linear ordinary differential equation (ODE)

$$\frac{d\sigma}{dt} = -\nu_1 \sigma(t) + C_1 \frac{\partial \sigma_e}{\partial t}(\lambda(t)), \quad \sigma(0) = 0. \tag{11}$$

The constants C_1 and ν_1 are unknown constants to be determined later; $\sigma_e(\lambda)$ is given in (5). Similarly, if we let $N = 2$, then $\sigma(t) = \epsilon_1(t) + \epsilon_2(t)$ and $G(t) \approx C_1 e^{-\nu_1 t} + C_2 e^{-\nu_2 t}$. The internal strain variables ϵ_1, ϵ_2 satisfy the following linear ODEs, respectively,

$$\frac{d\epsilon_1}{dt} = -\nu_1 \epsilon_1(t) + C_1 \frac{\partial \sigma_e}{\partial t}(\lambda(t)), \quad \epsilon_1(0) = 0 \tag{12}$$

$$\frac{d\epsilon_2}{dt} = -\nu_2 \epsilon_2(t) + C_2 \frac{\partial \sigma_e}{\partial t}(\lambda(t)), \quad \epsilon_2(0) = 0.$$

The parameters C_1, C_2, ν_1, and ν_2 are the corresponding unknown constants to be determined later. Considering the nonlinear dynamics formulation (10) with $N = 1$, we have in a third case $\sigma(t) = \epsilon_1(t)$ and σ is the solution of the following *nonlinear* ODE

$$\frac{d\sigma}{dt} = g(\sigma(t)) + K\frac{\partial \sigma_e}{\partial t}(\lambda(t)), \quad \sigma(0) = 0. \tag{13}$$

We assume that $g(z) = \sum_{i=1}^{4} a_i l_i(z)$ is a piecewise linear function of σ. In this case there are five constants to be determined: K, a_1, a_2, a_3, a_4.

To determine the effectiveness of the internal variable formulations, we compared the stress obtained numerically from each relation given above: Fung's stress-strain integral equation (3) using kernel (6), the ODE from using a one-exponential kernel (11), from using a two-exponential kernel (12), and the piecewise linear ODE (13). In each case, we set $u_x(x,t) = -m\sin(\omega t)$, with $m = 0.1$ and $\omega \in [100, 600]$, the frequency range of interest. Values for α and β were set as $\alpha = 0.1$ and $\beta = 1.0$ (see [6]). To compute Fung's kernel we set $c = 0.05$, $\tau_1 = 0.005$, and $\tau_2 = 50$ (again, see [6], [22]). We will assume, for the sake of comparison, that the constitutive equation from Fung is exact.

Each of the equations was solved numerically in MATLAB. For the integral expression we used an adaptive recursive Newton Cotes 8 panel rule. The ODEs were solved using the solver ODE15s, a variable order method for solving stiff ODEs. We initially set the unknown constants to values such that the corresponding kernels were decent approximations of Fung's kernel (6). The constants were then optimized using the Nelder-Mead simplex algorithm [14] so as to best approximate the σ obtained using Fung's kernel.

Figure 3 depicts the stresses $\sigma_i(t)$ obtained by each of the four constitutive equations with frequency $\omega = 600$Hz. Since the function is very oscillatory, we show $\sigma_i(t)$ only for $t \in [0.09, 0.1]$s. Figure 4 is the same plot, but over a smaller time interval to indicate more clearly the numerical differences. In each plot, σ obtained from Fung's method is indicated with a solid line labeled σ_{fung}, the one-exponential method is indicated with a dashed line (σ_{exp1}), the two-exponential method is indicated with a dashed-dot line (σ_{exp2}), and the nonlinear method is indicated with a dotted line (σ_{nl}).

The differences between σ using Fung's kernel and the alternate constitutive equations with optimized constants are slight. We emphasize that the unknown constants were optimized to match σ, *and not so that the exponential kernels best match Fung's kernel*. In general, more exponential terms in the kernel are needed to obtain good agreement with Fung's kernel.

We conclude from this numerical experiment that the alternate constitutive equations match quite well with Fung's stress-strain relation. Since the alternate relations are in differential form, the formulation is easy to implement and no longer requires the cumbersome storage of kernel history data. In the following sections we include the various stress-strain equations in the dynamic model and compare results with simulated data. First, we present the physical and
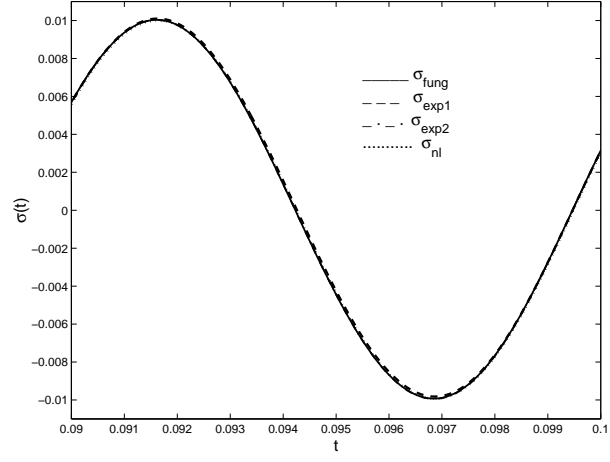
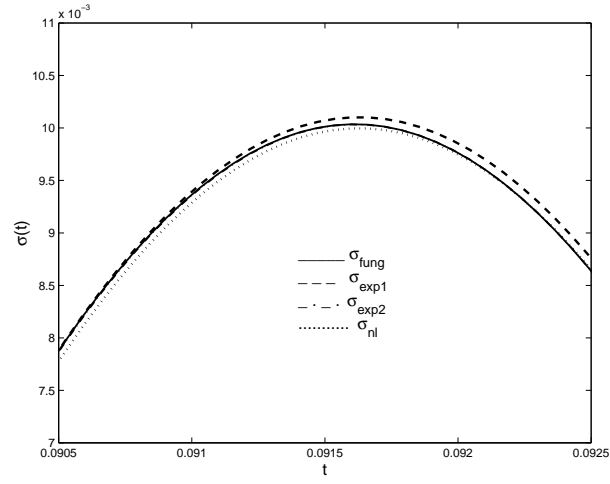8

Figure 3: Comparing $\sigma(t)$ with $\omega = 600$Hz.

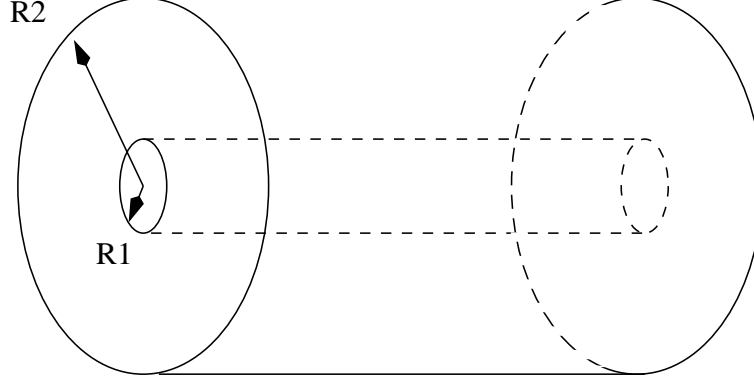Figure 4: Comparing $\sigma(t)$ with $\omega = 600$Hz (zoom).

9

Figure 5: The simplified physical model.

dynamic models, together with boundary and initial conditions, and discuss the numerical method used to integrate the models.

4 Physical and Dynamic Models

The simplified physical model is a cylindrical gel mold (such as those used in physical experiments at MedAcoustics) with a surgical tube passing through the center axisymmetrically. A source disturbance is generated within the tube. Shear waves propagate through the gel, and the shear displacement is measured (by sensors) at the gel outer surface. The gel possesses the material characteristics of soft tissue. The disturbance within the tube represents a source due to stenosis. Let R_1 and R_2 be the inner and outer radius of the gel, respectively. (see Figure 5). We assume that the source disturbance is time dependent, has only a radial component (i.e., it is axisymmetric), and the disturbance is a pure shear force. The outer surface of the gel is a free surface. The gel is initially at rest.

The one dimensional equations governing the shear stress $(\sigma(t, r))$ and shear displacement $(u(t, r))$ are

$$
\begin{aligned}
\rho \frac{\partial^2 u}{\partial t^2} &= \frac{\partial \sigma}{\partial r} \\
\sigma(t) &= \int_0^t G(t-s) \frac{\partial}{\partial s} \left(\beta e^{\alpha \partial_r u} \right) ds \\
\sigma(t, R_1) &= f(t), \qquad \sigma(t, R_2) = 0,
\end{aligned}
\tag{14}
$$

10

where $G(t)$ is Fung's reduced relaxation function, $\beta e^{\alpha \partial_r u}$ represents the elastic response, and $f(t)$ is the input shear stress. Since we are interested in the feasibility of a more computationally efficient stress-strain relation, we will not integrate the dynamic model with Fung's stress-strain relation.

Instead, in light of the simulation results for alternative stress formulations in the previous section, we concentrate on the internal strain variable constitutive relations. Using equation (11) as the stress-strain relation (i.e., $G(t) \approx C_1 e^{-\nu_1 t}$), we find that system (14) is equivalent to

$$
\begin{aligned}
\rho \frac{\partial^2 u}{\partial t^2} &= \frac{\partial \sigma}{\partial r} \\
\frac{\partial \sigma}{\partial t} &= -\nu_1 \sigma + C_1 \beta \frac{\partial}{\partial t}(e^{\alpha \partial_r u}) \\
\sigma(t, R_1) &= f(t), \qquad \sigma(t, R_2) = 0,
\end{aligned}
\tag{15}
$$

The unknown constants are C_1, ν_1, and α; since C_1 and β always appear as a product, we set $\beta = 1$ and let C_1 be the unknown constant. Using equation (12) as the stress-strain relation ($G(t) \approx C_1 e^{-\nu_1 t} + C_2 e^{-\nu_2 t}$), system (14) is equivalent to

$$
\begin{aligned}
\rho \frac{\partial^2 u}{\partial t^2} &= \frac{\partial}{\partial r}(\epsilon_1 + \epsilon_2) \\
\frac{\partial \epsilon_1}{\partial t} &= -\nu_1 \epsilon_1 + C_1 \beta \frac{\partial}{\partial t}(e^{\alpha \partial_r u}) \\
\frac{\partial \epsilon_2}{\partial t} &= -\nu_2 \epsilon_2 + C_2 \beta \frac{\partial}{\partial t}(e^{\alpha \partial_r u}) \\
\epsilon_1(t, R_1) &= \gamma f(t), \qquad \epsilon_1(t, R_2) = 0, \\
\epsilon_2(t, R_1) &= (1 - \gamma)f(t), \qquad \epsilon_2(t, R_2) = 0,
\end{aligned}
\tag{16}
$$

where $\sigma(t, r) = \epsilon_1(t, r) + \epsilon_2(t, r)$, and γ is a free parameter used to set the boundary conditions. The unknown constants in this system are C_1, C_2, ν_1, ν_2, and α. Finally, if we use the piecewise linear constitutive relation, equation (13), then we have the following nonlinear system

$$
\begin{aligned}
\rho \frac{\partial^2 u}{\partial t^2} &= \frac{\partial \sigma}{\partial r} \\
\frac{\partial \sigma}{\partial t} &= g(\sigma) + K \frac{\partial}{\partial t}(e^{\alpha \partial_r u}) \\
\sigma(t, R_1) &= f(t), \qquad \sigma(t, R_2) = 0,
\end{aligned}
\tag{17}
$$

where $g(\sigma) = \sum_{k=1}^{4} a_i l_i(\sigma)$ as before. The unknown constants are K, a_1, a_2, a_3, a_4, and α.

In the next section we describe the numerical method used to integrate each of the approximate systems.

11

5   Computational Methods

We use the same method to numerically integrate each of the approximate systems presented above. For simplicity, we present the method with respect to the one-exponential system given in (15); the two-exponential and piecewise linear systems are treated similarly.

First, we rewrite the (u, σ) system as a first order system in v, w, and μ where $v = \partial u / \partial t$, $w = \partial u / \partial r$, and $\mu = \sigma - C \beta e^{\alpha w}$ (or $\mu_i = \epsilon_i - C_i \beta e^{\alpha w}$). The corresponding (v, w, μ) system for system (15) is

$$
\begin{aligned}
\frac{\partial \mu}{\partial t} &= -\nu_1 (\mu + C_1 \beta e^{\alpha w}) \\
\frac{\partial v}{\partial t} &= \frac{1}{\rho} \frac{\partial}{\partial r} (\mu + C_1 \beta e^{\alpha w}) \\
\frac{\partial w}{\partial t} &= \frac{\partial v}{\partial r},
\end{aligned}
\tag{18}
$$

which is now in conservative form and is essentially hyperbolic.

Physical boundary conditions are prescribed in terms of σ, but are translated into boundary conditions for w by analytically integrating the stress-strain equation in system (15) over $(0, t)$, and solving for $w(t, r)$ at the boundaries ($r = R_1$ and $r = R_2$). The boundary conditions for w are then

$$
\begin{aligned}
w(t, R_1) &= \frac{1}{\alpha} \ln \left(\frac{f(t) - f(0) + C_1 \beta e^{\alpha w(0, R_1)} + \nu_1 \int_0^t f(s)\, ds}{C_1 \beta} \right) \\
w(t, R_2) &= w(0, R_2).
\end{aligned}
$$

Since the gel is initially at rest, the initial conditions are $v(0, r) = 0$, $w(0, r) = 0$, and $\mu(0, r) = -C_1 \beta$.

To numerically integrate the system, subject to the above boundary and initial conditions, we employ a MacCormack finite difference scheme which is second-order in space and time. Boundary conditions for v and μ are updated using local direction cosines at the domain boundaries (see, e.g., [13] or [24] on hyperbolic systems). If the local direction points into the domain, then the update uses the new boundary data (i.e., $w(t^{n+1}, R_1)$ or $w(t^{n+1}, R_2)$). Otherwise, the local direction points out of the domain, and boundary values are updated using data from the domain interior and second-order differences to approximate any spatial derivatives.

The stability of the method is verified through a Von Neumann analysis of the linearized (μ, v, w) system about the initial condition. We apply the MacCormack scheme to the linearized model and then substitute in planar waves of the form $v = \hat{v} e^{i(kr + \omega t)}$, $w = \hat{w} e^{i(kr + \omega t)}$, and $\mu = \hat{\mu} e^{i(kr + \omega t)}$. Let $\chi = e^{i \omega \Delta t}$ be the amplification factor, and let $\theta = j \Delta r$, $\tau = \Delta t / \Delta r$ and $\gamma = C \beta \alpha / \rho$.

Nontrivial solutions for $\hat{\mu}, \hat{v}, \hat{w}$ imply the following condition for χ,

$$(\chi - 1)\left[(\chi - 1)^2 + (\chi - 1)\left\{\nu\Delta t(1 - \frac{\nu\Delta t}{2}) + 2\tau^2\gamma(1 - \cos\theta)\right\}\right.$$

$$+\tau^2\gamma\left\{\nu\Delta t(1 - \frac{\nu\Delta t}{2})(1 - \cos\theta) + (\tau^2\gamma\frac{\nu^2\Delta t^2}{4})(1 - \cos\theta)^2\right.$$

$$\left.\left.+(1 - \frac{\nu\Delta t}{2})^2\sin^2\theta\right\}\right] = 0.$$

Solving this expression for χ, we have $\chi = 1$, or

$$\chi = 1 - \tau^2\gamma(1\cos\theta) - \frac{\nu\Delta t}{2}(1 - \frac{\nu\Delta t}{2})$$

$$\pm \sqrt{\frac{\nu^2\Delta t^2}{4}(1 - \frac{\nu\Delta t}{2})^2 - \frac{\nu^2\Delta t^2}{4}\tau^2\gamma(1 - \cos\theta)^2 - \tau^2\gamma(1 - \frac{\nu\Delta t}{2})^2\sin^2\theta}$$

The scheme is stable when $|\chi| \leq 1$. Since χ depends on seven parameters: C, ν, α, β, ρ, $\Delta t/\Delta r$, and Δt, we easily check the stability of the scheme for a particular parameter set using the above expression for χ, rather than determine a domain of stability. For the computational experiments described in the next section, we verified that the parameter set produces a stable scheme.

We performed a grid refinement to verify the second-order accuracy of the scheme. This was done with the forced (μ, v, w) system by choosing an exact solution and setting the forcing functions appropriately. We chose the following exact solutions for u and σ,

$$u(t, r) = -m(1 - \cos(\omega t))\left(\frac{r - R_1}{R_2 - R_1}\right)^2, \qquad \sigma(t, r) = m\sin(\omega t)\left(\frac{R_2 - r}{R_2 - R_1}\right),$$

where m is the oscillation amplitude, and ω is the oscillation frequency. For these calculations, $m = 0.1$ and $\omega \in [100, 600]$ Hz. The exact solutions for the (μ, v, w) system are calculated as $\mu = \sigma - C\beta e^{\alpha u_r}$, $v = u_t$, and $w = u_r$.

To perform the grid refinement, we fix the ratio $\frac{\Delta t}{\Delta r}$ and repeatedly halve the time step and the spatial increment. The truncation error for each variable is computed as the L_∞ norm of the difference between the exact and numerical solutions. For example, the truncation error for μ is

$$E_n(\mu) = \|\mu(T, r_i) - \mu_i^N\|_\infty$$

where $\mu(T, r_i)$ and μ_i^N are the exact and numerical solutions, respectively, at the point (T, r_i). The superscript $N = T/\Delta t$ indicates the number of numerical time increments, and $r_i = R_1 + i\Delta r$, $i = 1, \ldots, N_r$, represents the spatial grid points. The subscript n indicates the level of refinement; initially $n = 0$. With each refinement, we increment n and double the total number of time steps (N) and the number of grid points (N_r). Setting $\frac{\Delta t}{\Delta r} = 1/20\text{sm}^{-1}.$, $T = 5\text{s}$, $R_2 - R_1 = 1\text{m}.$, and $N_r = 40$ for the initial convergence test, we compute the ratio $E_n(\cdot)/E_{n+1}(\cdot)$ for each state variable. The results for v are given below.

13

Table 1: Grid Refinement Analysis for v

n	$||E_n(v)||_\infty$	$||E_n(v)||_\infty / ||E_{n+1}(v)||_\infty$
0	0.1295	
1	0.0321	4.03
2	0.0080	4.01
3	0.0020	4.00
4	5.0054e-04	3.99

A ratio of 4 indicates the code is second order accurate. Results for w, and μ are similar.

Hence the scheme is indeed stable and second-order accurate. In the next section we will compare this system, as well as the two exponential and piecewise linear systems, with published data.

6 Model Simulations

To measure the ability of the approximate systems to match experimental data, we compare the results of the dynamic models presented in Section 4 with simulation data derived from the experimental results of Verburg. This is a first step in the ultimate goal of matching shear displacement data measured on the the outer surface of the gel.

In [26] Verburg presents wave speeds per frequency for shear waves propagating through a homogeneous medium with mechanical properties similar to the lung tissue located between the heart valves and the chest wall. Output data is generated from the Verburg data in the following way. First, the input signal is a sum of weighted sine waves with a sampling rate of 12288 Hz and $\Delta f = 6$ Hz. Using the Verburg wave speeds, a phase shift is calculated for each input frequency. The output signal is then the weighted sum of sine waves with velocity phase delays. The resulting simulation data does not account for attenuation due to damping or dispersion loss. Also, the input and output data sets are the same order derivative in time. Since the dynamic model expects input shear stress, we interpret the simulation data as force in (scaled by a constant) and acceleration out (see Figure 6 for a graph of the input function).

To compare the model with this simulated data, we solve the associated best fit inverse problem. In other words, we make an initial guess for the unknown constants in the model, then optimize the constants using the Nelder-Mead algorithm. The Nelder-Mead cost function is the L_2 norm of the difference of the simulated output data and the model acceleration data at the outer boundary $(r = R_2)$. The model acceleration data is generated by solving the forward problem, i.e, by numerically integrating the dynamic model. Note, the acceleration data is obtained as a finite difference approximation of $\partial v / \partial t$.

In Figures 7-9 we compare the simulated Verburg data and the optimized dynamic model data. Each figure contains two plots. The top plot compares
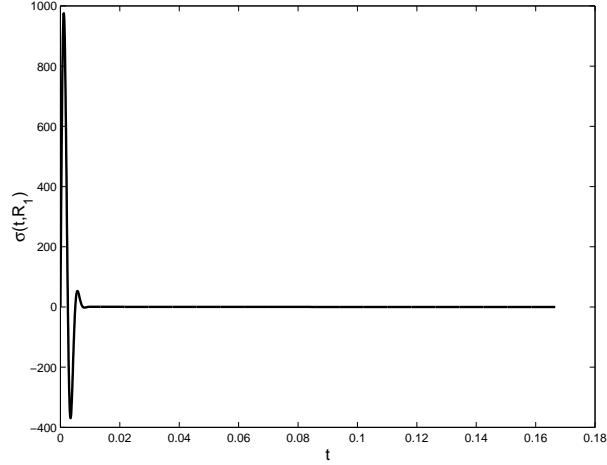
14

Figure 6: The input shear stress function $\sigma(t, R_1) = f(t)$.

the normalized acceleration data (normalized since the simulated data does not account for dissipation). The bottom plot compares the normalized fast Fourier transform (FFT) of the output data. This plot indicates which frequencies are excited by each model. In all plots, the simulated Verburg data is indicated with a solid line; the model data is indicated with a dashed line.

Figure 7 exhibits data from the one-exponential system (15), Figure 8 presents data from the two-exponential system (16), and data from the piecewise linear system (17) is shown in Figure 9.

Note that the unknown constants are optimized only with respect to the acceleration data. That is, the fit-to-data uses the acceleration data; the FFT of the optimized model is then compared to the FFT of the data. Any additional matching of the FFT data is an independent indicator that the alternate models are reasonable. In each case the optimized systems achieve the correct time lag in the acceleration data. None of the model simulations contain the small oscillations that appear for $t > 0.03$s, probably because the internal strain variable models contain dissipation whereas the simulated data does not. Clearly, the optimized two-exponential model produces the best approximation with the simulated data; differences in this case are nearly indiscernible.

7 Conclusions

In the case of simple one-dimensional shear wave propagation through a homogeneous soft tissue (viscoelastic) medium, we have demonstrated that dynamic
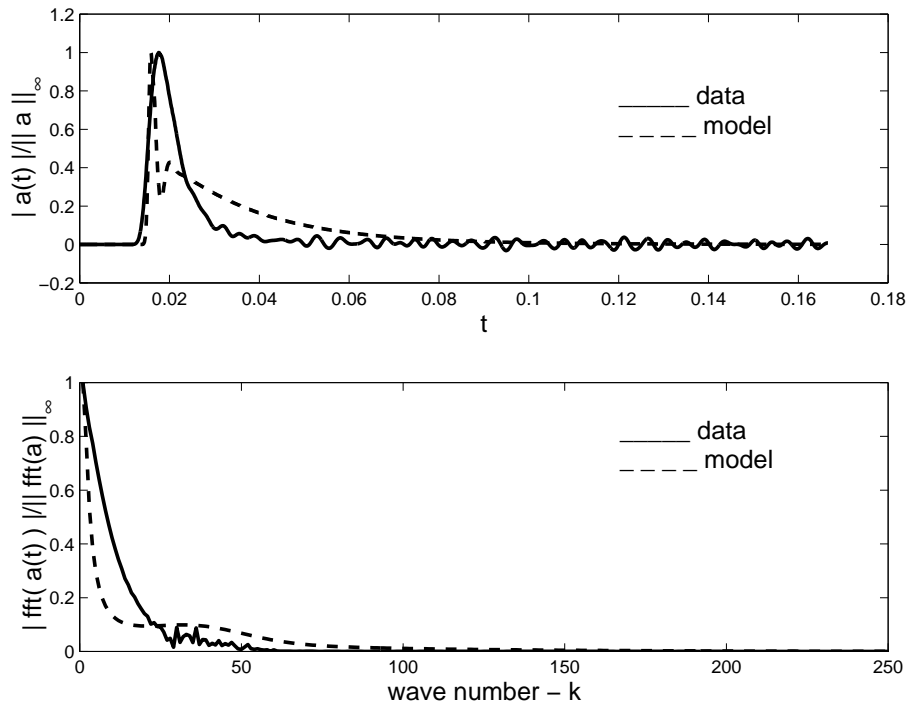
15

Figure 7: Comparison with the one-exponential system.
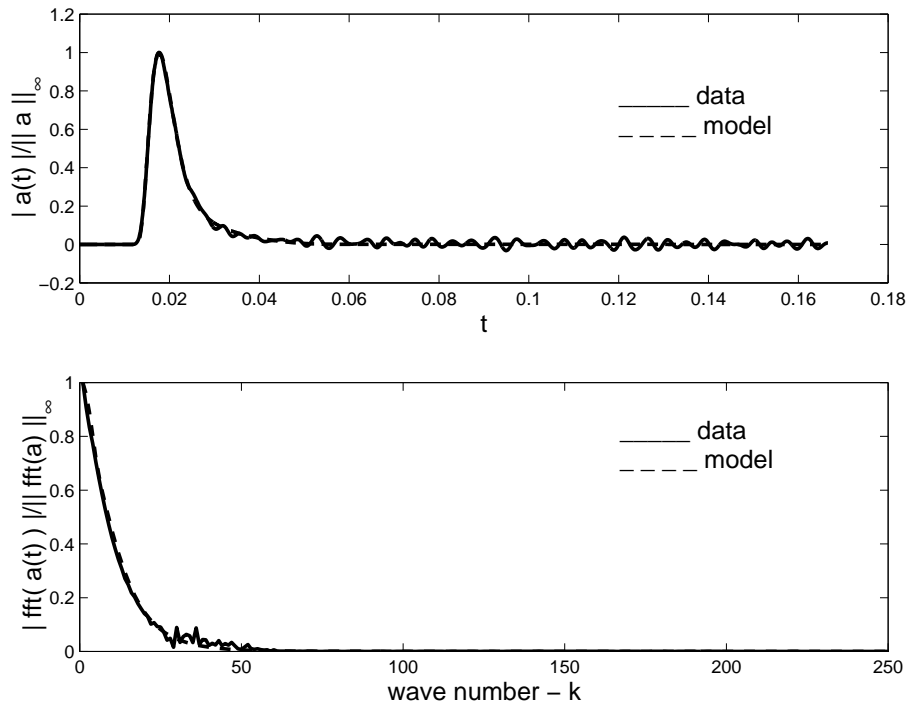
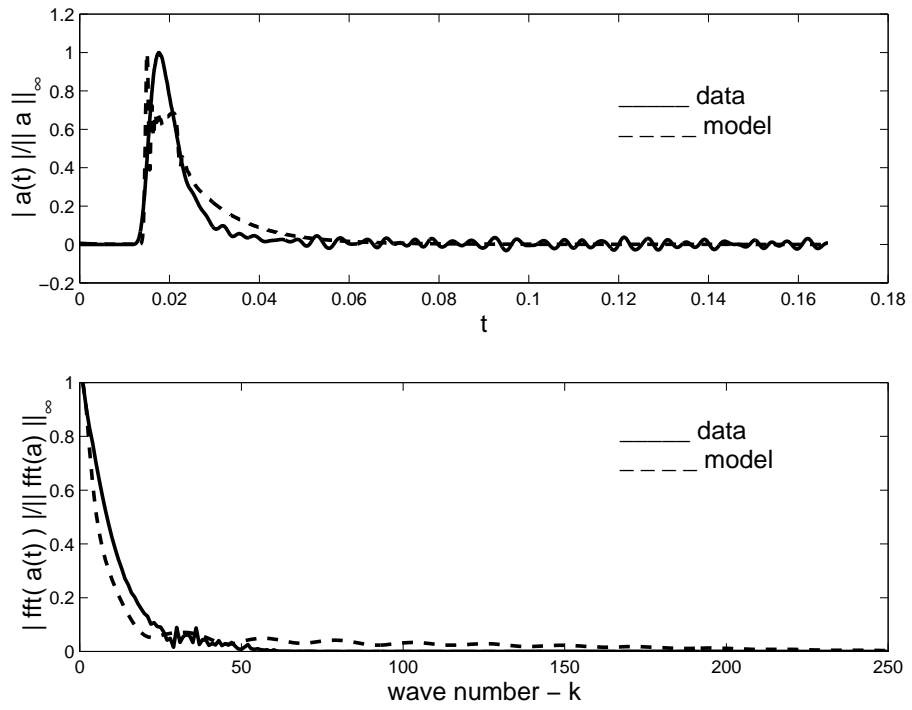Figure 8: Comparison with the two-exponential system.

Figure 9: Comparison with the piecewise linear system.

simulation using an internal variable based constitutive relation matches well with data. Moreover, the internal strain variable formulations lead to systems of first order differential equations, rather than an integro-differential model, making the alternate models more computationally tractable. It should be noted that these alternate constitutive relations may not match well with Fung's relation (3) in all respects of viscoelastic behavior. However, the main goal in the efforts reported here is to match shear displacement data after propagation through a soft tissue-like medium. In this respect, the optimized models with internal variable strain formulations are, we believe, adequate. The one and two-exponential models correspond to standard kernel formulations in viscoelastic theory (i.e., a finite series of Kelvin models). It is quite possible that the simulated Verburg data does not capture all nonlinear behavior that might be present in complex experimental data. Hence our models with *linear* internal dynamics and *nonlinear* coupling with the infinitesimal strain produce a good fit to this data. However we also achieve decent agreement between data and the model with *nonlinear* internal dynamics (as represented by the piecewise linear model), which offers promise for use of this class of models with more complex data. Future efforts will include modeling of the two-dimensional propagation problem. In this case there is a variety of experimental data available to be employed in model validation.

8   Acknowledgments

References

[1] M. Akay, Noninvasive detection of coronary artery disease using advanced signal processing methods, PhD. dissertation, Rutgers University, Piscataway, NJ 1990.

[2] American Heart Association, 1999 heart and stroke statistical update, *American Heart Association*, 1998.

[3] H.T. Banks, G.A. Pinter, L.K. Potter, M.J. Gaitens, and L.C. Yanyo, "Modeling of quasi-static and dynamic load responses of filled viscoelastic materials", CRSC-TR98-48, Raleigh, NC, December 1998; *Modeling: Case Studies from Industry*, (E. Cumberbatch and A. Fitt, eds.), Cambridge Univ. Press., to appear.

[4] H.T. Banks, G.A. Pinter, L.K. Potter, B.C. Munoz, and L.C. Yanyo, "Estimation and control related issues in smart material structures and fluids",

CRSC-TR98-2, Raleigh, NC, January 1998; *Opt. Techniques and Applications*, (L. Caccetta, et. al., eds.), Curtain Univ. Press, p. 19-34, 1998.

[5] Y.L. Chen and Y.C. Fung, Stress-strain history relations of rabbit mesentery in simple elongation, *Biomechanical Symposium, ADM-2, ASME*, 1973, 9–10.

[6] L.J.M.G. Dortmans, A.A.H.J. Sauren, and E.P.M. Rousseau, Parameter estimation using the quasi-linear viscoelastic model proposed by Fung, Trans. of the ASME, *J. Biomech. Engr.*, **106**, 1984, 198–202.

[7] Y.C. Fung, *A First Course in Continuum Mechanics* Prentice-Hall, Inc., New Jersey, (1977).

[8] Y.C. Fung, *Biomechanics: Mechanical Properties of Living Tissues* Springer-Verlag, New York, (1993).

[9] J.E. Galbraith, M.L. Murphy, and N. de Soyza, Coronary angiogram interpretation. Interobserver variability, *Jama*, **240**, 1978, 2053–2056.

[10] R.C. Haut and R.W. Little, A constitutive equation for collagen fibers, *J. Biomechanics*, **5**, 1972, 423–430.

[11] R. B. Jenkins and R.W. Little, A constitutive equation for parallel-fibered elastic tissue, *J. Biomechanics*, **7**, 1974, 397–402.

[12] A.R. Johnson, A. Tessler, and M. Dambach, "Dynamics of thick elastic beams", *J. Engr. Materials and Tech.*, **119**, 1997, 273–278.

[13] J. Kevorkian, *Parital Differential Equations: Analytical Solution Techniques*, Wadsworth, Inc., California, (1990).

[14] J.C. Lagarias, J.A. Reeds, M.H Wright, and P.E. Wright, Convergence properties of the Nelder-Mead simplex method in low dimensions, *SIAM J. Optim.*, **9**, 1999, 112–147.

[15] MedAcoustics Inc., internal documentation. Raleigh, NC.

[16] I. Nigul and U. Nigul, On algorithms of evaluation of Fung's relaxation function parameters, *J. Biomechanics,* **20**, 1987, 343–352.

[17] S.E. Nissen and J.C. Gurley, Application of intravascular ultrsound for detection and quantitation of coronary atherosclerosis, *Int. J. Cardiac Imaging*, **6**, 1991, 165–177.

[18] N.L. Owsley and A.J. Hull, Beamformed nearfield imaging of a simulated coronary artery containing a stenosis, *IEEE Trans. Med. Imaging*, **17**, 1998, 900–909.

[19] J.G. Pinto and P.J. Patitucci, Visco-elasticity of passive cardiac muscle, *ASME J. Biomechanical Eng.*, **102**. 1980, 57–61.

[20] E.P.M. Rousseau, A.A.H.J Sauren, M.C. van Hout, and A.A. van Steenhoven, Elastic and viscoelastic material behavior of fresh and gluteraldehyde-treated porcine aortic valve tissue, *J. Biomechanics*, **16**, 1983, 339-348.

[21] A.A.H.J. Sauren, M.C. van Hout, A.A. van Steenhoven, F.E. Veldpaus, and J.D. Janssen, The mechanical properties of porcine aortic valve tissues, *J. Biomechanics*, **16**, 1983, 327–338.

[22] A.A.H.J. Sauren and E.P.M. Rousseau, A concise sensitivity analysis of the quasi-linear viscoelastic model proposed by Fung, *ASME J. Biomechanical Eng.*, **105**, (1983), 92–95.

[23] J.L. Semmlow, W. Welkowitz, J. Kostis and J.W. MacKenzie, Coronary artery disease correlates between diastolic auditory characteristics and coronary artery stenoses, *IEEE Trans. Biomed. Eng.*, **BME-30**, 1983, 136–139.

[24] J.C. Strickwerda, *Finite Difference Schemes and Partial Differential Equations*, Wadsworth, Inc., California, (1989).

[25] T.T. Tanaka and Y.C. Fung, Elastic and inelastic properties of the canine aorta and their variation along the aortic tree, *J. Biomechanics*, **7**, 1974, 357–370.

[26] J. Verburg, Transmission of vibrations of the heart to the chestwall, *Adv. Cardiovasc. Phys.* **5**, 1983, 84–103.

[27] J. Verburg and E. van Vollenhoven, Phonocardiography: Physical and technical aspect and clinical uses, in *Noninvasive Physiological Measurements* (ed. P. Rolfe), Academic Press, London, (1979).

[28] S.L.Y. Woo, B.R. Simon, S.C. Huei, and W.H. Akeson, Quasi-linear viscoelastic properties of normal articular cartilage, *ASME J. Biomechanical Eng.*, **102**, 1980, 85–90.

[29] S.L.Y. Woo, M.A. Gomez, and W.H. Akeson, The time and history-dependent viscoelastic properties of the canine medial collateral ligament, *ASME J. Biomechanical Eng.*, **103**, 1981, 293–298.

[30] S.L.Y. Woo, Mechanical properties of tendons and ligaments: I. Quasi-static and nonlinear viscoelastic properties, *Biorheology*, **19**, 1982, 385–396.